

Transport at the border between Gauss and Lévy universality classes

Lior Zarfaty,¹ Alexander Peletskyi,^{2,3} Itzhak Fouxon,¹ Sergey Denisov,^{2,4} and Eli Barkai¹

¹*Department of Physics, Institute of Nanotechnology and Advanced Materials, Bar-Ilan University, Ramat-Gan, 52900, Israel*

²*Institute of Physics, University of Augsburg, Universitätsstrasse 1, D-86135, Augsburg Germany*

³*Sumy State University, Rimsky-Korsakov Street 2, 40007 Sumy, Ukraine*

⁴*Department of Applied Mathematics, Lobachevsky State University of Nizhny Novgorod, Gagarina Av. 23, Nizhny Novgorod, 603950, Russia*

A wide range of physical systems, from cold atoms diffusing in an optical lattice to bacteria undergoing random motion, can be tuned to operate at the transition point between the Gauss and Lévy limiting laws. Here we investigate such dynamics using the Lorentz gas with infinite horizon, where this kind of behavior appears naturally. We obtain Lambert scaling of the particles' packet which captures the dynamics of these systems on finite time scales, while the rigorous $t \rightarrow \infty$ results are practically unreachable due to logarithmically slow convergence. In contrast to the Gaussian center part of the packet, we show that its outskirts are described by a universal power law, as these systems belong neither to the Gauss nor to the Lévy domains of attraction. Further, the underlying symmetry of the lattice on which the scatterers are arranged is imprinted in the spreading packet's shape, thus showing significant deviations from normal diffusion.

The central limit theorem explains the omnipresence of diffusion phenomena, which appear in science and various aspects of life. The theorem establishes that the sum of properly scaled independent identically distributed (IID) random variables tends towards a normal/Lévy distribution, when the variables' variance is finite/infinite, respectively. Here we investigate the problem exactly at the transition point, between the well-known normal and Lévy limiting laws. Diffusive systems operating at this point exhibit rich physics, in the sense of a critical slowing down and a dual nature of the transport, as they do not actually belong to either one of the two classes. This case includes one of the oldest transport models, the so-called Lorentz gas with infinite horizon [1, 2], in which a point-like tracer moves at a constant speed, while undergoing elastic collisions with fixed scatterers [3–15]. Our goal is to quantitatively describe this marginal behavior.

We address two dynamical models, which represent a classical approach to transport characterized by this borderline behavior: a one-dimensional channel of stadium billiards, and a set of circular scatterers on a two-dimensional square lattice, see Fig. 1. The free path in these systems is unbounded and hence the models are called the infinite horizon Lorentz gases (see Ref. [16] for a review). We also consider a simple stochastic representation of this behavior: a sum of IID random variables $\{\chi_n\}$ drawn from a symmetric though fat tailed probability density function (PDF) $f(\chi)$, with $f(\chi \gg 1) \propto \chi^{-3}$. It sits at the transition between the Gauss and Lévy domains of attraction, in the sense that a PDF $f(\chi)$ with lighter/heavier tails belong to the Gaussian/Lévy families, respectively.

In an infinite horizon Lorentz gas, a particle's trajectory exhibits the phenomenon of intermittency. Namely, the particle undergoes epochs of diffusive-like behavior with many random reorientations, after which it follows an almost ballistic path within the endless corridors, see

Fig. 1. For the two-dimensional Lorentz billiards, Bleher [17] showed that $\lim_{t \rightarrow \infty} [\mathbf{r}(t) - \mathbf{r}(0)] / \sqrt{t \ln(t)}$ is a Gaussian variable, i.e. the diffusive packet's width grows logarithmically faster than normal (see also Ref. [18]). However, this limit theorem hides the physically observable nature of the process [19], since it is valid only when $\ln[\ln(N)] / \ln(N) = \epsilon \ll 1$ where N is the number of collisions, and as such even if N is very large we may argue that this condition is not really satisfied (for example, $\epsilon = 0.01 \Rightarrow N \approx 10^{281}$). Moreover, as illustrated in a simulation of the stadium channel model, Fig. 2b, the particles' density in its far tail is described by a power law, clearly deviating from a Gaussian. Therefore, our goal is to present a theory which: I) captures the packet's dynamics on physically attainable time scales, and II) describes correctly the tails of the PDF, thus extending the mathematical results valid for the center when $t \rightarrow \infty$. To do so, we go beyond the Gaussian description, and use below what we call a Lambert scaling approach, which solves the logarithmic convergence problem. We also show that the underlying geometry of the array of scatterers is imprinted in the diffusing packet's shape. We quantify these anomalous features using analytical methods and numerical simulations.

Fat-tailed waiting times. The infinite corridors in the Lorentz systems lead to exceptionally long travel times $\{\tau_n\}$ between collision events, for which the $\text{PDF}(\tau)$ follows a fat tailed law, $\psi(\tau) \propto \tau^{-3}$ when τ is large [20, 21]. Thus, the variance of $\psi(\tau)$ diverges, but just marginally. The particle's displacement is $\mathbf{r}(t) - \mathbf{r}(0) = \sum_{n=1}^N \mathbf{v}_{n-1} \tau_n + \mathbf{v}_N \tau^*$. Here N is the random number of collisions till time t , τ_n is the walking time of the n -th travel epoch, \mathbf{v}_n with $n \geq 1$ is the velocity just after the n -th collision, \mathbf{v}_0 and $\mathbf{r}(0)$ are the initial velocity and displacement which are both randomly chosen, and the last travel event is of duration $\tau^* = t - \sum_{n=1}^N \tau_n$. During this process the particle's speed is fixed due to the elasticity

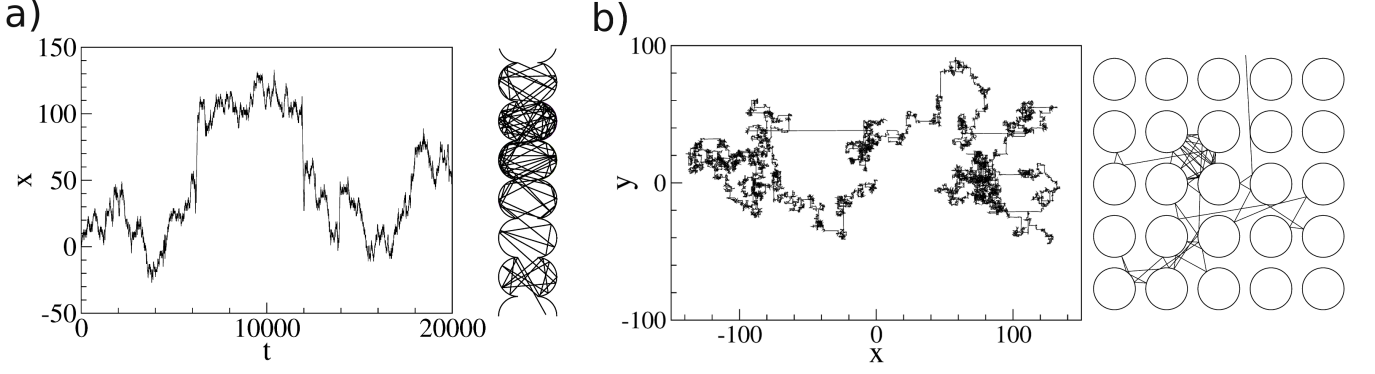


FIG. 1. In a Lorentz gas, a particle is moving with a constant speed, elastically colliding with periodically arranged semicircle walls - billiard channel model (a) and scatterers residing on a square lattice - Lorentz model (b). Notice the long flights along the infinite corridors. In the simulations we used a semicircles' radius of 1 with walls separation of unity (billiard channel), and $R = 0.4$ for the radius of the scatterers with a lattice constant of unity (Lorentz model).

of the collisions, and we choose $V = |\mathbf{v}_n| = 1$.

Central limit theorem at the transition between Lévy and Gauss phases. Since the waiting times between collision events in the infinite horizon Lorentz gas are power-law distributed, we are motivated to first investigate a simpler problem. Therefore, we consider a sum of $N \gg 1$ IID random variables, $x = \sum_{n=1}^N \chi_n$, where the summands are drawn from a common PDF $f(\chi) = f(-\chi)$ and $f(\chi \rightarrow \infty) \simeq \chi_0^2/\chi^3$. Here N and $\{\chi_n\}$ roughly correspond to the measurement time divided by the mean time between collisions, $t/\langle\tau\rangle$, and the lengths of inter-collision travel, $\{\mathbf{v}_{n-1}\tau_n\}$, respectively. We define the scaled sum as $\bar{x} = x/\sqrt{\chi_0^2 N \Omega(N)/2}$ with $N\Omega(N)$ being a scaling function. We use the characteristic function

$$\langle \exp(i\bar{k}\bar{x}) \rangle = \exp \left\{ N \ln \left[\tilde{f} \left(\frac{\bar{k}}{\sqrt{\chi_0^2 N \Omega(N)/2}} \right) \right] \right\}, \quad (1)$$

where $\tilde{f}(k)$ is the Fourier transform of $f(\chi)$. Assuming that $\Omega(N)$ monotonically increases with N , the small k behavior of $\tilde{f}(k)$ is considered [22]:

$$\tilde{f}(k) \simeq 1 + \frac{1}{2} (\chi_0 k)^2 \ln \left[(C_f \chi_0 k)^2 \right]. \quad (2)$$

The first term is the normalization, while the second is related to the power-law tail of $f(\chi)$, with C_f being:

$$C_f = \exp \left\{ \gamma - \frac{3}{2} - \int_0^{\chi_0} d\chi f(\chi) \left(\frac{\chi}{\chi_0} \right)^2 \right. \quad (3) \\ \left. - \int_{\chi_0}^{\infty} d\chi \left[f(\chi) \left(\frac{\chi}{\chi_0} \right)^2 - \frac{1}{\chi} \right] \right\},$$

where $\gamma \approx 0.5772$ is Euler's constant. Inserting this expression into Eq. (1) and expanding, we get

$$\langle \exp(i\bar{k}\bar{x}) \rangle \simeq \exp \left\{ \frac{\bar{k}^2}{\Omega(N)} \ln \left[\frac{2C_f^2 \bar{k}^2}{N \Omega(N)} \right] \right\}. \quad (4)$$

We now determine the slowly increasing function $\Omega(N)$ with the choice $\ln[N\Omega(N)/(2C_f^2)] = \Omega(N)$, which yields:

$$\Omega(N) = \left| W_{-1} \left(-\frac{2C_f^2}{N} \right) \right|. \quad (5)$$

Here $W_{-1}(\eta)$ is the secondary branch of the Lambert W-function [23], defined for $\eta \in [-1/e, 0)$ by the identity $W_{-1}(\eta) = \ln[\eta/W_{-1}(\eta)]$. The Lambert function has the following expansion as $\eta \rightarrow 0^-$:

$$|W_{-1}(\eta)| = L_1 + L_2 + \frac{L_2}{L_1} + \mathcal{O} \left(\frac{L_2^2}{L_1^2} \right), \quad (6)$$

where $L_1 = \ln(1/|\eta|)$ and $L_2 = \ln[\ln(1/|\eta|)]$. By virtue of Eqs. (5) and (6), one has $N\Omega(N) \simeq N \ln(N)$ when $N \rightarrow \infty$, and thus the sum x scales like $\sqrt{N \ln(N)}$ which is a well-known result. However, the convergence to this mathematical limit is ultra-slow, and the aforementioned Lambert scaling approach cures this problem for any *reasonably* large N . We now expand Eq. (4) for large $\Omega(N)$:

$$\langle \exp(i\bar{k}\bar{x}) \rangle \simeq e^{-\bar{k}^2} \left[1 + \frac{\bar{k}^2}{\Omega(N)} \ln(\bar{k}^2) \right]. \quad (7)$$

Inverting Eq. (7) back to position space, we reach our first main result, the PDF of x :

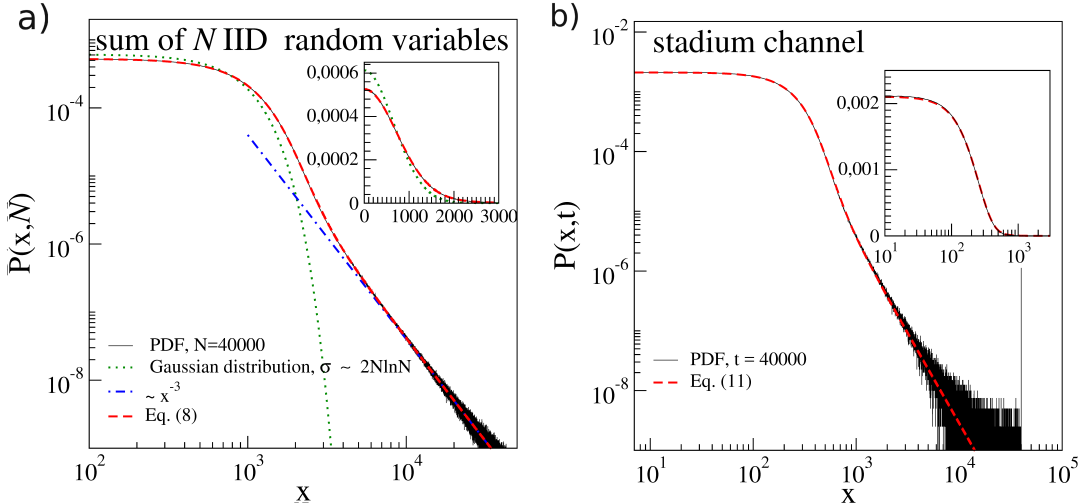


FIG. 2. (color online) The PDF of a sum of N IID random variables (a) with $f(\chi) = |\chi|^{-3}$ for $|\chi| > 1$, while 0 otherwise, and the density for the channel of stadium billiards (b). These models are well described by the Lambert scaling, the Kummer correction, and a clear transition between a Gaussian center to a power law tail. The well-known $N \ln(N)$ -scaled Gaussian fails to describe the sum's PDF even for a large N , see the inset in (a). The theory Eq. (11) fits nicely to the model of the stadium billiards, with higher resolution of the center part given in the inset of (b). The Kummer correction is important for an accurate description of the power law tail.

$$P(x, N) \simeq \frac{1}{\sqrt{\pi \xi^2(N)}} \exp \left[-\frac{x^2}{\xi^2(N)} \right] \left\{ 1 + \frac{1}{\Omega(N)} \left\{ \left[2 - \gamma - \ln(4) \right] \left[\frac{1}{2} - \frac{x^2}{\xi^2(N)} \right] - \frac{1}{2} M^{(1,0,0)} \left[-1; \frac{1}{2}; \frac{x^2}{\xi^2(N)} \right] \right\} \right\}, \quad (8)$$

with $\xi(N) = \sqrt{2\chi_0^2 N \Omega(N)}$. Here $M(\dots)$ is Kummer's confluent hypergeometric function [23] and the superscript over M denotes its derivative with respect to its first argument.

As said above, the Lambert function's leading order yields for Eq. (8) the known result, namely that $P(x, N)$ is a Gaussian with width $\sim \sqrt{N \ln(N)}$. However, considering the correction to this leading order presented in Eq. (6), we see that reaching this limit demands $\ln(N) \gg \ln[\ln(N)]$, and as mentioned in the introduction this is not practical. In addition, the Kummer function's term in Eq. (8) yields for large x the power law behavior $P(x, N) \propto |x|^{-3}$. It follows that the Lambert scaling and Kummer correction found here are a required necessity for a numerical analysis, as seen in Fig. 2a. The $|x|^{-3}$ decay clearly stems from the original summands' PDF, which has a far tail of $f(\chi) \propto |\chi|^{-3}$. Our analysis thus shows the precise way in which the Gaussian center of the PDF changes into the power law statistics.

Our goal now is to show that the Lambert scaling and the power law tail decay of the scaled sum of IID random variables can also be used to describe the probability distribution of particles in the infinite horizon Lorentz gases. We note that the case of summation just considered has two obvious drawbacks. First, the model does not take into consideration the finite velocity of the particle. Physically, a particle initially on the origin cannot

be found beyond the circle $|\mathbf{r}| = Vt$, and for this reason we expect a sharp cutoff on the power-law tail just obtained. Secondly, in dimension higher than one we must take into consideration the scatterers' geometry. These problems are now resolved using the Lévy walk approach, which sets a finite speed and anisotropy due to geometry.

Using the Lévy walk approach [24–26], we define a process where the waiting times $\{\tau_n\}$ are IID random variables drawn from the fat tailed PDF, $\psi(\tau \rightarrow \infty) \simeq \tau_0^2/\tau^3$. Similarly, the velocities \mathbf{v}_n after each collision (or renewal) are drawn from a PDF we denote $F(\mathbf{v})$. For the two-dimensional Lorentz billiards we set the lattice constant to unity. It can be shown from simple geometrical arguments that when the scatterers' radius obeys $1/\sqrt{8} < R < 1/2$, one has a couple of perpendicular open horizons stretching to infinity, creating the cross-like density profile shown in Fig. 3. Out of these considerations, we use a velocity model which is aligned along the lattice's axes, and since the speed is unity we have $F_2(\mathbf{v}) = \{[\delta(v_x-1) + \delta(v_x+1)]\delta(v_y) + \delta(v_x)[\delta(v_y-1) + \delta(v_y+1)]\}/4$. Similarly, for the one-dimensional stadium channel model we use $F_1(v) = [\delta(v-1) + \delta(v+1)]/2$. Let $P(\mathbf{r}, t)$ be the Lévy walkers' PDF, all starting from a common origin at $\mathbf{r}(0) = 0$, and let $\Pi(\mathbf{k}, u)$ be its Fourier-Laplace transform, $\{\mathbf{r} \rightarrow \mathbf{k}, t \rightarrow u\}$. Since this stochastic model describes a renewal process, reflecting the chaotic nature of the collision events, we apply the well-known Montroll-

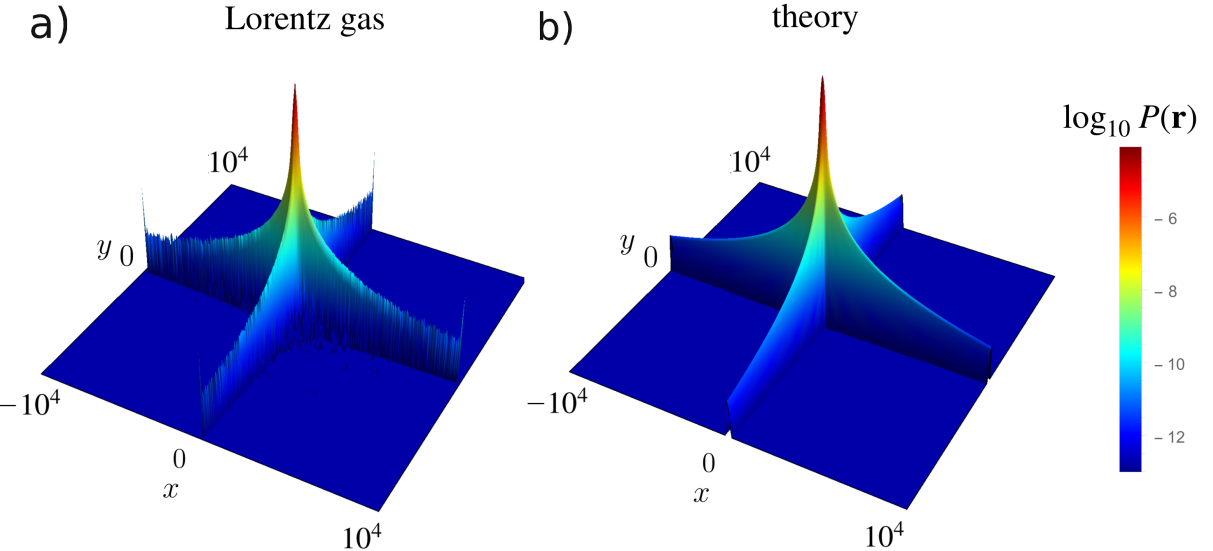


FIG. 3. (color online) The PDF for the Lorentz gas with two open horizons yields a cross-like symmetry, where the simulation depicted is of duration $t = 10^4$ (a). This non-Gaussian shape clearly illustrates the sensitivity of the spreading density to the underlying structure of the square lattice of scatterers. The theoretical approximation Eq. (11) (b) is in agreement with the simulation (see also cross sections along the lines $y = 0$ and $y = x$ and further details on data analysis in [22]).

Weiss approach [25]

$$\Pi(\mathbf{k}, u) = \left\langle \frac{1 - \hat{\psi}(u - i\mathbf{k} \cdot \mathbf{v})}{u - i\mathbf{k} \cdot \mathbf{v}} \right\rangle \frac{1}{1 - \langle \hat{\psi}(u - i\mathbf{k} \cdot \mathbf{v}) \rangle}, \quad (9)$$

where $\langle \dots \rangle$ in the above equation are averages with respect to the velocity's PDF, and $\hat{\psi}(u)$ is the Laplace transform of $\psi(\tau)$. To invert this equation in the long time limit, one needs to consider the small u behavior of $\hat{\psi}(u)$, which is [22]:

$$\hat{\psi}(u) \simeq 1 - \langle \tau \rangle u - \frac{1}{2} (\tau_0 u)^2 \ln(C_\psi \tau_0 u) + o(u^2), \quad (10)$$

where C_ψ is defined similarly to C_f in Eq. (3). In Eq. (10), the first term is normalization, while the last arises from the fat tail asymptotics of $\psi(\tau)$.

The packet of spreading particles, in the long time limit, in dimension $d = 1$ (one-dimensional stadium channel) and $d = 2$ (two-dimensional Lorentz gas), is found with an asymptotic small $\{\mathbf{k}, u\}$ expansion of Eq. (9) [22]:

$$P(\mathbf{r}, t) \simeq \left[\frac{1}{\pi \xi^2(t)} \right]^{d/2} \exp \left[-\frac{r^2}{\xi^2(t)} \right] \left\{ 1 + \frac{1}{\Omega(t)} \sum_{j=1}^d \left\{ \left[2 - \gamma - \ln(4) \right] \left[\frac{1}{2} - \frac{r_j^2}{\xi^2(t)} \right] - \frac{1}{2} M^{(1,0,0)} \left[-1; \frac{1}{2}; \frac{r_j^2}{\xi^2(t)} \right] \right\} \right\}, \quad (11)$$

where

$$\begin{aligned} \xi(t) &= \Xi \sqrt{\frac{t}{T^d} \Omega(t)}, & \Xi &\equiv 2C_\psi \tau_0 V, \\ \Omega(t) &= \left| W_{-1} \left(-\frac{T^d}{t} \right) \right|, & T &\equiv 4C_\psi^2 \langle \tau \rangle, \end{aligned} \quad (12)$$

when in our case $V = 1$, as mentioned. This solution is shown in Figs. 2b ($d = 1$) and 3 ($d = 2$), together with a sampling of the corresponding billiard systems. These figures illustrate how the Lambert scaling and power law tail of the density remain a valid description

beyond the simpler case considered above, i.e. a summation of IID random variables. The Kummer functions provide a power law decay of the density proportional to $|x|^{-3}$ and $|y|^{-3}$ along the corresponding axes. Two scale factors, Ξ and T , enter in the solution Eq. (11) and are found by numerically fitting it to a $t = 10^4$ simulation. The solution's stability was then checked by performing simulations for longer times. Considering extremely long time durations for Eq. (11), namely t for which $\Omega(t) \simeq \ln(t)$, yields a Gaussian profile with a variance of $\sigma_G^2 t \ln(t)$, where $\sigma_G^2 = \Xi^2 / 2T$. Focusing on the

Lorentz gas system, Bleher [17] showed rigorously that the limit $\lim_{t \rightarrow \infty} [\mathbf{r}(t) - \mathbf{r}(0)]/\sqrt{t \ln(t)}$ converges in distribution to a Gaussian variable with zero mean, and a variance which is given by the scatterers' radius as (see also Ref. [20]):

$$\sigma_G^2 = \frac{2(1-2R)^2}{\pi(1-\pi R^2)}. \quad (13)$$

Quantitatively comparing our numerical result with this theoretical prediction, we receive an agreement with a relative error of $\sim 1\%$ [22]. Basically, it means that this theory has only one free parameter instead of two, as the relation $\Xi^2/2T$ can be determined from Eq. (13).

In [16], an interesting doubling effect was pointed out. While for familiar normal processes, e.g. Brownian motion, the Gaussian packet's variance is equal to the mean square displacement (MSD), in our case there exists a factor of 2 between them. It arises from the process' fat tail behavior, as the MSD has two contributing elements, the Gaussian bulk and the far tail $\sim |\mathbf{r}|^{-3}$. As only half of the MSD can be explained using the Gaussian approximation, one needs to go beyond it. In this sense, the power law tail obtained in this letter is needed for a correct description of the MSD, which is the standard quantifier of diffusive processes. Calculating the MSD demands the introduction of a far tail cutoff, namely the density is zero beyond $|\mathbf{r}| = t$ (see Figs. 2b and 3). In order to receive a full description of the problem, one must construct a theory moving from that end point $|\mathbf{r}| = t$ inward, e.g. the infinite covariant density [27].

Discussion and summary. Our theory captures processes which are on the borderline between Gauss and Lévy domains of attraction. Recalling Fig. 2a, it greatly extends the $N \ln(N)$ -scaled Gaussian's regime of accuracy. Furthermore, it can be used to predict the far tail behavior of systems for which computer simulations are challenging and time consuming to handle [19]. While the rigorous $t \ln(t)$ -scaled Gaussian limit was clearly a breakthrough [16–18], it does not capture the universal power law fall of the tail exhibited here.

Lambert scaling and the special behaviors found here are general features of systems working at the border between Gauss and Lévy universality classes. For atoms in shallow optical lattices it was shown, both theoretically and experimentally, that the dynamics exhibits a transition from Gauss to Lévy laws, which is controlled by the intensity of the lasers [28, 29]. Thus, in that case, one can tune the system to work at the transition point, and the behaviors found in this work are expected to be applicable. Scale free networks have a degree distribution $P(k) \sim k^{-\gamma}$, with $\gamma \approx 3$ in several cases. This indicates that a behavior near the vicinity of the Lévy-Gauss transition is natural, as the too narrow/wide Gauss/Lévy regime, respectively, might be non-optimal (see also empirical data sets in Ref. [30]). Another example for critical statistics are Hamiltonian systems with sharply di-

vided phase space (mushroom billiards etc.) [31], and models of bacteria flow where a certain aspect ratio is tuned to the transition [32]. While here we studied the critical point itself, working in the vicinity of it might reveal similar behaviors.

Acknowledgments. This work was supported by the Israel Science Foundation grant No. 1898/17 (LZ, IF and EB). Numerical simulations were supported by the Russian Science Foundation grant No. 16-12-10496 (SD).

- [1] L. A. Bunimovich, *Zh. Eksp. Teor. Fiz.* **89**, 1452-1471 (1985).
- [2] L. A. Bunimovich, Ya. G. Sinai, and N. I. Chernov, *Russian Math. Surveys* **45**:3 105-152 (1990).
- [3] N. Friedman, A. Kaplan, D. Carasso, and N. Davidson, *Phys. Rev. Lett.* **86**, 1518 (2001).
- [4] D. Armstead, B. R. Hunt, and E. Ott, *Phys. Rev. Lett.* **89** 284101 (2002).
- [5] D. N. Armstead, B. R. Hunt, and E. Ott, *Phys. Rev. E.* **67**, 021110 (2003).
- [6] R. Artuso and G. Cristadoro, *Phys. Rev. Lett.* **90**, 244101 (2003).
- [7] G. M. Zaslavsky and M. A. Edelman, *Physica D* **193**, 128-147 (2004).
- [8] P. Bálint and S. Goüzel, *Comm. Math. Phys.* **263**, 461 (2006).
- [9] D. P. Sanders and H. Larralde, *Phys. Rev. E*, **73**, 026205 (2006).
- [10] M. Courbage, M. Edelman, S. M. Saberi Fathi, and G. M. Zaslavsky, *Phys. Rev. E*, **77**, 036203 (2008).
- [11] D. I. Dolgopyat, and N. L. Chernov, *Russ. math. Surv.* **64**, 651, (2009).
- [12] R. Burioni, L. Caniparoli, and A. Vezzani, *Phys. Rev. E.*, 060101(R) (2010).
- [13] G. Cristadoro, T. Gilbert, M. Lenci, and D. P. Sanders, *Phys. Rev. E* **90**, 050102 (2014).
- [14] A. Bianchi, G. Cristadoro, M. Lenci, and M. Ligabó, *J. Stat. Phys.* **163** 22 (2016).
- [15] M. Spanner, F. Höfling, S. C. Kapfer, K. R. Mecke, G. E. Schröder-Turk, and T. Franosch, *Phys. Rev. Lett.* **116**, 0606601 (2016).
- [16] C. P. Dettmann, *J. Stat. Phys.* **146**, 181 (2012).
- [17] P. M. Bleher, *J. Stat. Phys.* **66**, 1-2 (1992).
- [18] D. Saász and T. Varjú, *J. Stat. Phys.* **129**, 59 (2007).
- [19] G. Cristadoro, T. Gilbert, M. Lenci, and D. P. Sanders, *Phys. Rev. E* **90**, 022106 (2014).
- [20] J. P. Bouchaud and P. Le Doussal, *J. Stat. Phys.* **41**, 225 (1985).
- [21] A. Zachar, T. Geisel, J. Nierwetberg, and G. Radons, *Phys. Lett. A* **114**, 317 (1986).
- [22] Included in the supplementary material.
- [23] As defined in <http://functions.wolfram.com>, November 9, 2017.
- [24] M. F. Shlesinger, B. J. West, and J. Klafter, *Phys. Rev. Lett.* **58**, 1100 (1987).
- [25] V. Zaburdaev, S. Denisov, and J. Klafter, *Rev. Mod. Phys.* **87**, 483 (2015).
- [26] V. Zaburdaev, I. Fouxon, S. Denisov, and E. Barkai, *Phys. Rev. Lett.* **117**, 270601 (2016).

- [27] A. Rebenshtok, S. Denisov, P. Hänggi, and E. Barkai, *Phys. Rev. Lett.* **112**, 110601 (2014).
- [28] D. A. Kessler, and E. Barkai, *Phys. Rev. Lett.* **108**, 230602 (2012).
- [29] Y. Sagi, M. Brook, I. Almog, and N. Davidson, *Phys. Rev. Lett.* **108**, 093002 (2012).
- [30] A. Clauser, C. R. Shalizi, and M. E. J. Newman, *SIAM Review* **51**, 661-703 (2009).
- [31] E. G. Altmann, A. E. Motter, and H. Kantz, *Phys. Rev. E* **73**, 026207 (2006).
- [32] G. Ariel, A. Beer, and A. Reynolds, *Phys. Rev. Lett.* **118**, 228102 (2017).

SUPPLEMENTARY MATERIAL

Leading behavior of $\hat{\psi}(u \rightarrow 0)$

Here we derive Eq. (10), obtaining Eq. (3) during the process. We omit the derivation of Eq. (2), as it can be done similarly to the following. Let us assume that $\psi(\tau)$ behaves asymptotically as

$$\lim_{\tau \rightarrow \infty} \psi(\tau) \tau^3 = \tau_0^2, \quad \tau_0 > 0, \quad (14)$$

with its Laplace transform being defined by

$$\hat{\psi}(u) = \int_0^\infty d\tau \psi(\tau) e^{-u\tau}. \quad (15)$$

We will now show that using Eq. (14), Eq. (15) reduces to Eq. (10) for small u . To do so, we rewrite Eq. (15) as:

$$\hat{\psi}(u) = 1 - u \langle \tau \rangle + \int_0^\infty d\tau \psi(\tau) \left[e^{-u\tau} - 1 + u\tau \right]. \quad (16)$$

In order to find the leading behavior of the last term of Eq. (16), the following limit is considered:

$$l_1 = \lim_{u \rightarrow 0} \frac{1}{u^2 \ln(u)} \int_0^\infty d\tau \psi(\tau) \left[e^{-u\tau} - 1 + u\tau \right]. \quad (17)$$

Using L'Hospital's rule three times, followed by a change of variable to $\eta = u\tau$, Eq. (17) takes the form:

$$l_1 = -\frac{1}{2} \lim_{u \rightarrow 0} \int_0^\infty d\eta \psi\left(\frac{\eta}{u}\right) \left(\frac{\eta}{u}\right)^3 e^{-\eta}. \quad (18)$$

For any finite u , the integrand vanishes for $\eta = 0$, as $\psi(\tau)$ is normalized. Since a finite set of bounded points does not contribute to an integral, we may discard this point, such that the integration is carried over the domain $(0, \infty)$. This allows us to employ the dominated convergence theorem, and switch the order of limit and integration in Eq. (18). Together with Eq. (14), we have:

$$l_1 = -\frac{\tau_0^2}{2} \int_{0^+}^\infty d\eta e^{-\eta} = -\frac{\tau_0^2}{2}, \quad (19)$$

which shows that the limit $l_1 = -\tau_0^2/2$ is finite, yielding:

$$\hat{\psi}(u) \simeq 1 - \langle \tau \rangle u + l_1 u^2 \ln(u) + \mathcal{O}(u^2). \quad (20)$$

To complete the derivation, we calculate the next order correction $\sim u^2$. For that cause, the following limit is considered:

$$l_2 = \lim_{u \rightarrow 0} \frac{1}{u^2} \left\{ \int_0^\infty d\tau \psi(\tau) \left[e^{-u\tau} - 1 + u \langle \tau \rangle \right] d\tau + \frac{\tau_0^2}{2} u^2 \ln(u) \right\}. \quad (21)$$

Using L'Hospital's rule two times, followed by a split of the integral at $\tau = \tau_0$, l_2 becomes:

$$l_2 = \frac{1}{2} \lim_{u \rightarrow 0} \int_0^{\tau_0} d\tau \psi(\tau) \tau^2 e^{-u\tau} + \frac{1}{2} \lim_{u \rightarrow 0} \left\{ \int_{\tau_0}^\infty d\tau \psi(\tau) \tau^2 e^{-u\tau} + \tau_0^2 \left[\ln(u) + \frac{3}{2} \right] \right\}. \quad (22)$$

The first integral of Eq. (22) is carried over a finite region, so one can exchange the order of limit and integration. From the second integral, we add and subtract the term τ_0^2/τ^3 from $\psi(\tau)$, which yields:

$$l_2 = \frac{1}{2} \int_0^{\tau_0} d\tau \psi(\tau) \tau^2 + \frac{1}{2} \lim_{u \rightarrow 0} \int_{\tau_0}^\infty d\tau \left[\psi(\tau) - \frac{\tau_0^2}{\tau^3} \right] \tau^2 e^{-u\tau} + \frac{1}{2} \lim_{u \rightarrow 0} \left\{ \int_{\tau_0}^\infty d\tau \frac{\tau_0^2}{\tau} e^{-u\tau} + \tau_0^2 \left[\ln(u) + \frac{3}{2} \right] \right\}. \quad (23)$$

Note that due to the asymptotics Eq. (14), the second integral in Eq. (23) converges when $u \rightarrow 0$. Evaluating the upper row limit and the lower row integral, we obtain:

$$l_2 = \frac{1}{2} \int_0^{\tau_0} d\tau \psi(\tau) \tau^2 + \frac{1}{2} \int_{\tau_0}^\infty d\tau \left[\psi(\tau) - \frac{\tau_0^2}{\tau^3} \right] \tau^2 + \frac{1}{2} \lim_{u \rightarrow 0} \tau_0^2 \left[\Gamma(0, \tau_0 u) + \ln(u) + \frac{3}{2} \right], \quad (24)$$

where $\Gamma(\cdot, \cdot)$ is the incomplete Gamma function, which has the small parameter behavior $\Gamma(0, \eta) \simeq -\ln(\eta) - \gamma + \eta$. Thus, after some algebra one finds for Eq. (21):

$$l_2 = -\frac{\tau_0^2}{2} \ln(C_\psi \tau_0), \quad (25)$$

where the constant C_ψ is defined in Eq. (3) with the following changes: $\{f \rightarrow \psi, \chi \rightarrow \tau, \chi_0 \rightarrow \tau_0\}$. Equation (10) then follows from:

$$\hat{\psi}(u) \simeq 1 - \langle \tau \rangle u + l_1 u^2 \ln(u) + l_2 u^2 + o(u^2). \quad (26)$$

A similar calculation can be performed on the Fourier transform of the PDF $f(\chi)$, which results in Eq. (2) and C_f .

Bulk approximation of the Lévy walk model with Lambert scaling

The d -dimensional Lévy-walk model is defined as follows: a random walker is placed at $\mathbf{r}(0)$ on time $t = 0$. Its movement consists of segments of ballistic motion with constant velocity, separated by collision-like events which induce a change in the velocity's magnitude and/or direction. The process lasts for a predetermined time duration (the measurement time t). The model employs two PDFs in order to determine the displacement during each of the ballistic motion epochs. The velocity of each segment is drawn from a PDF $F(\mathbf{v})$, whose moments are all finite, and is further assumed to be symmetric with respect to each of the components v_j , with $1 \leq j \leq d$, such that its odd moments vanish. The time duration of each ballistic section is drawn from a PDF $\psi(\tau)$. The movement continues until the allotted measurement time is met, thus the number of collisions N in $(0, t)$ is random. This yields the total displacement as:

$$\mathbf{r}(t) - \mathbf{r}(0) = \sum_{n=1}^N \mathbf{v}_{n-1} \tau_n + \mathbf{v}_N \tau^*, \quad (27)$$

with $0 \leq \tau^* = t - \sum_{n=1}^N \tau_n$. The traveling times and velocities $\{\tau_n, \mathbf{v}_n\}$, for $1 \leq n \leq N$, are IID random variables, and the initial conditions $\mathbf{r}(0)$ and \mathbf{v}_0 are drawn from equilibrium. Let us denote the probability to find the walker at a position \mathbf{r} on time t as $P(\mathbf{r}, t)$. Applying Fourier and Laplace transforms to the spatial and temporal coordinates of $P(\mathbf{r}, t)$ respectively, an exact expression of the probability in Fourier-Laplace space, denoted $\Pi(\mathbf{k}, u)$, is given by the Montroll-Weiss equation (9), where

$$\langle \dots \rangle \equiv \int_{-\infty}^{\infty} d^d v F(\mathbf{v}) \dots . \quad (28)$$

As mentioned in the text, in order to find the density of particles while accounting for the problem's spatial structure, we take for the stadium channel ($d = 1$) and the Lorentz billiards ($d = 2$) the following velocity PDFs:

$$F_1(v) = \frac{1}{2} \left[\delta(v - V) + \delta(v + V) \right], \quad (29)$$

and:

$$F_2(\mathbf{v}) = \frac{1}{4} \left\{ \left[\delta(v_x - V) + \delta(v_x + V) \right] \delta(v_y) + \delta(v_x) \left[\delta(v_y - V) + \delta(v_y + V) \right] \right\}, \quad (30)$$

respectively, where $V > 0$ is a constant (in the main text

$V = 1$). This yields for Eq. (9)'s denominator:

$$1 - \left\langle \hat{\psi}(u - i\mathbf{k} \cdot \mathbf{v}) \right\rangle = \frac{1}{2d} \sum_{j=1}^d \left[\hat{\psi}(u - iV k_j) + \hat{\psi}(u + iV k_j) \right]. \quad (31)$$

In order to use the asymptotic form (10), let us assume a scaling of $u \sim k^2 L(|\mathbf{k}|)$, where $L(\cdot)$ is some logarithmic-behaving function. This suggests that $u \ll V|\mathbf{k}|$ when $|\mathbf{k}| \rightarrow 0$. Using the identity

$$\ln(a \pm ib) = \frac{1}{2} \ln(a^2 + b^2) \pm i \arctan\left(\frac{b}{a}\right) \quad (32)$$

together with Eq. (10), while neglecting the appropriate terms according to the above scaling assumption, one has

$$\begin{aligned} \hat{\psi}(u \pm iV k_j) &\simeq 1 - \langle \tau \rangle (u \pm iV k_j) \\ &\quad - \frac{1}{4} (\tau_0 V k_j)^2 \ln \left[(C_\psi \tau_0 V k_j)^2 \right] \pm i \frac{\pi}{4} (\tau_0 V k_j)^2. \end{aligned} \quad (33)$$

Plugging this into Eq. (31) while discarding irrelevant terms with respect to the above scaling assumption, we get for the denominator of Eq. (9):

$$\begin{aligned} 1 - \left\langle \hat{\psi}(u - i\mathbf{k} \cdot \mathbf{v}) \right\rangle &\simeq \\ &u \langle \tau \rangle - \frac{1}{4d} \sum_{j=1}^d (\tau_0 V k_j)^2 \ln \left[(C_\psi \tau_0 V k_j)^2 \right], \end{aligned} \quad (34)$$

while for its numerator we have:

$$\left\langle \frac{1 - \hat{\psi}(u - i\mathbf{k} \cdot \mathbf{v})}{u - i\mathbf{k} \cdot \mathbf{v}} \right\rangle \simeq \langle \tau \rangle. \quad (35)$$

Therefore we find, using Eq. (9):

$$\Pi(\mathbf{k}, u) \simeq \left[u - \frac{\tau_0^2 V^2}{4d \langle \tau \rangle} \sum_{j=1}^d k_j^2 \ln \left(C_\psi^2 \tau_0^2 V^2 k_j^2 \right) \right]^{-1}. \quad (36)$$

Returning to the time domain yields for the Fourier transform of $P(\mathbf{r}, t)$:

$$\tilde{P}(\mathbf{k}, t) \simeq \exp \left[t \frac{\tau_0^2 V^2}{4d \langle \tau \rangle} \sum_{j=1}^d k_j^2 \ln \left(C_\psi^2 \tau_0^2 V^2 k_j^2 \right) \right]. \quad (37)$$

Defining $\kappa = \mathbf{k} \sqrt{\tau_0^2 V^2 t \Omega(t) / (4d \langle \tau \rangle)}$, where $\Omega(t)$ is a yet unknown scaling function, leads to:

$$\begin{aligned} \tilde{P}(\kappa, t) &\simeq \\ &\left[\frac{4d \langle \tau \rangle}{\tau_0^2 V^2 t \Omega(t)} \right]^{d/2} \exp \left\{ \sum_{j=1}^d \frac{\kappa_j^2}{\Omega(t)} \ln \left[\frac{4d C_\psi^2 \langle \tau \rangle}{t \Omega(t)} \kappa_j^2 \right] \right\}. \end{aligned} \quad (38)$$

Demanding that $\ln[t\Omega(t)/(4dC_\psi^2\langle\tau\rangle)] = \Omega(t)$ yields:

$$\Omega(t) = \left| W_{-1} \left(-4dC_\psi^2 \frac{\langle\tau\rangle}{t} \right) \right|, \quad (39)$$

thus we obtain the following form for (38):

$$\begin{aligned} \tilde{P}(\boldsymbol{\kappa}, t) &\simeq \quad (40) \\ \left[\frac{4d\langle\tau\rangle}{\tau_0^2 V^2 t \Omega(t)} \right]^{d/2} e^{-\kappa^2} \exp \left[\sum_{j=1}^d \frac{\kappa_j^2}{\Omega(t)} \ln(\kappa_j^2) \right] &\simeq \\ \left[\frac{4d\langle\tau\rangle}{\tau_0^2 V^2 t \Omega(t)} \right]^{d/2} e^{-\kappa^2} \left[1 + \sum_{j=1}^d \frac{\kappa_j^2}{\Omega(t)} \ln(\kappa_j^2) \right]. \end{aligned}$$

The assumption of large t constricts us to large $\Omega(t)$, so the second exponential term is expanded to sub-leading order. The inverse Fourier transform is:

$$P(\mathbf{r}, t) = \int \frac{d^d \kappa}{(2\pi)^d} \tilde{P}(\boldsymbol{\kappa}, t) \cos \left[\frac{\boldsymbol{\kappa} \cdot \mathbf{r}}{\tau_0 V} \sqrt{\frac{4d\langle\tau\rangle}{t\Omega(t)}} \right]. \quad (41)$$

Evaluating these integrals, the leading and sub-leading orders of Eq. (41) result in Eqs. (11) and (12). The MSD can be calculated from differentiating the Montroll-Weiss Eq. (9). We find that in the long time limit:

$$\langle r^2(t) \rangle \simeq \tau_0^2 V^2 \frac{t}{\langle\tau\rangle} \left[\ln \left(\frac{t}{C_\psi \tau_0} \right) - 2 + \gamma \right]. \quad (42)$$

Details of the simulations and fitting procedure

To verify that this new approximation matches the stadium channel and Lorentz billiards models, we checked whether the two parameters Ξ and T are identical for two different times. We first noticed that Eq. (11) is analytically integrable, with the following primitive function:

$$\begin{aligned} \mathcal{P}(\mathbf{r}, t) &= \left(\prod_{j=1}^d \int_0^{r_j} dr'_j \right) P(\mathbf{r}', t) \simeq \left\{ \prod_{j=1}^d \frac{1}{2} \operatorname{erf} \left[\frac{r_j}{\xi(t)} \right] \right\} \\ &\times \left\{ 1 + \frac{1}{\sqrt{\pi}\Omega(t)} \sum_{j=1}^d \frac{r_j}{\xi(t)} \frac{\exp[-r_j^2/\xi^2(t)]}{\operatorname{erf}[r_j/\xi(t)]} \right. \\ &\times \left. \left\{ 2 - \gamma - \ln(4) - M^{(1,0,0)} \left[0; \frac{3}{2}; \frac{r_j^2}{\xi^2(t)} \right] \right\} \right\}. \quad (43) \end{aligned}$$

For the channel model ($d = 1$), we used a simulation of duration $t = 10^4$, which had a lattice constant of length

2, i.e. the semicircles' radius is 1. The bins' index was defined as $n = \text{floor}[(x+1)/2]$, where $\text{floor}(\eta)$ gives the greatest integer less than or equal to η . We used Wolfram Mathematica's FindFit function, with a fitting model of $\mathcal{P}_{\text{bin}}(n, t) = \mathcal{P}(2n+1, t) - \mathcal{P}(2n-1, t)$, which represents the total probability of finding a particle in the n -th bin. From this fitting procedure we got, using the first 101 bins ($0 \leq n \leq 100$), that $\xi(10^4) \approx 126$ and $\Omega(10^4) \approx 11.2$, which correspond to $\Xi \approx 0.463$ and $T \approx 1.51$, for time $t = 10^4$. We then used these results to predict $P(x, t)$ for a time duration of $t = 4 \cdot 10^4$ (Fig. 2 in the main text).

For the billiards model ($d = 2$), we used a simulation of duration $t = 10^4$, which had a billiard radius of $R = 0.4$ and a lattice constant of unity. The bins' indexes were defined as $n = \text{int}(x/50)$ and $m = \text{int}(y/50)$, where $\text{int}(\eta)$ is the integer part of η . Notice that in this case the $(0, 0)$ bin has twice the area of an $(n > 0, 0)$ bin and four times the area of an $(n > 0, m > 0)$ bin, therefore the appropriate histogram values were divided by a relevant factor. We used Wolfram Mathematica's FindFit function, with a model of $\mathcal{P}_{\text{bin}}(n, m, t) = \mathcal{P}(50n+50, 50m+50, t) + \mathcal{P}(50n, 50m, t) - \mathcal{P}(50n+50, 50m, t) - \mathcal{P}(50n, 50m+50, t)$, which represents all/half/quarter of the probability to find a particle in the $(n > 0, m > 0)/(n > 0, 0)/(0, 0)$ bin, respectively. We performed a one-dimensional fit by setting $m = 0$. Using the first 101 bins ($0 \leq n \leq 100$), we obtained $\xi(10^4) \approx 116$ and $\Omega(10^4) \approx 26.4$, which correspond to $\Xi \approx 2.17 \cdot 10^{-4}$ and $T \approx 4.66 \cdot 10^{-7}$, for time $t = 10^4$. We then used these results to predict $P(x, t)$ for a time duration of $t = 4 \cdot 10^4$ (not shown). Furthermore, it follows from the rigorous results Eq. (13) that:

$$\frac{\Xi^2}{2T} = \frac{2(1-2R)^2}{\pi(1-\pi R^2)}, \quad (44)$$

while using Eq. (42) and Eq. (12), we obtain:

$$\lim_{t \rightarrow \infty} \frac{\langle r^2(t) \rangle}{t \ln(t)} = \frac{\tau_0^2 V^2}{\langle\tau\rangle} = \frac{\Xi^2}{T}. \quad (45)$$

Plugging in the numbers and comparing the two sides of Eq. (44), we get an excellent agreement, while the doubling effect can be seen from comparing it to Eq. (45). The simulation's mean time between collisions, $\langle\tau\rangle_S \approx 0.6213$, was found to be consistent with the analytical expression [16]:

$$\langle\tau\rangle_A = \frac{1 - \pi R^2}{2R} \approx 0.6217. \quad (46)$$

Finally, cross sections of $\mathcal{P}_{\text{bin}}(n, m, t)$ are depicted in Fig. 4, for $m = 0$ (a) and $m = n$ (b), which roughly correspond to $y = 0$, and $y = x$.